Increasing dust emission from ice free terrain in southeastern Greenland since 2000

Tomomi Amino[1,2,†], Yoshinori Iizuka[1*], Sumito Matoba[1], Rigen Shimada[3], Naga Oshima[4], Toshitaka Suzuki[5], Takuto Ando[6], Teruo Aoki[7] and Koji Fujita[8*],

1: Institute of Low Temperature Science, Hokkaido University, Kita 19-jo Nishi 8-chome, Kita-ku, Sapporo, 060-0819, Japan

2: Graduate School of Environmental Science, Hokkaido University, Kita 10-jo Nishi 5-chome, Kita-ku, Sapporo, 060-0810, Japan

3: Earth Observation Research Center, Japan Aerospace Exploration Agency, 2-1-1, Sengen, Tsukuba, Ibaraki 305-8505, Japan

4: Meteorological Research Institute, 1-1 Nagamine, Tsukuba, Ibaraki 305-0052, Japan

5: Faculty of Science, Yamagata University, 1-4-12 Kojirakawa, Yamagata 990-8560, Japan

6: Arctic Research Center, Hokkaido University, Kita 21-jo Nishi 11-chome, Kita-ku, Sapporo, 060-0819, Japan

7: National Institute of Polar Research, 10-3, Midori-cho, Tachikawa-shi, Tokyo 190-8518, Japan

8: Graduate School of Environmental Studies, Nagoya University, F3-1(200) Furo-cho, Chikusa-ku, Nagoya 464-8601, Japan

*Corresponding author: Yoshinori Iizuka (iizuka@lowtem.hokudai.ac.jp) and Koji Fujita (cozy@nagoya-u.jp)

†present address: ORGANO Corporation, 1-2-8 Shinsuna, Koto-ku, Tokyo, 136-8631, Japan

Highlight

- Annual and seasonal dust fluxes during 1960–2014 are reconstructed from an ice core of the southeastern dome in Greenland (SE-Dome).
- The annual dust fluxes are high after 2000 primarily due to increasing dust flux during autumn.
- Local dust emissions increased after 2000 due to a warming-induced increase in snow-free land on Greenland's east coast.

Abstract

Mineral dust plays a key role in both local and global climates. At high latitudes, atmospheric dust can affect ice-nuclei formation, and surface dust can reduce the albedo as well as increase subsequent ice melting. As a proxy for past climate,

mineral dust is preserved in ice cores, but few studies have examined deposited dust in ice cores during the Anthropocene, especially after 2000. We measured dust concentrations in an ice core at the southeastern dome in Greenland (SE-Dome), and reconstructed the annual and seasonal dust fluxes during 1960–2014. We find the annual average flux during 1960–2014 to be 34.8 ± 13.5 mg m^{-2} yr^{-1}, a value about twice that of ice cores further inland. The more recent part of that period, 2000–2014, has the higher annual flux of 46.6 ± 16.2 mg m^{-2} yr^{-1}. The annual and autumn dust fluxes highly correlate with air temperature in Tasiilaq (r = 0.61 and 0.50, respectively), a coastal location in southeastern Greenland. Our results suggest that the local dust emissions at the coastal region are increasing due to a decreasing seasonal snow-cover area arising from coastal Greenland warming after 2000.

Keyword: Greenland, dust, ice core, annual flux, seasonal flux

1 Introduction

Mineral dust has global and local effects on climate (Carslaw et al., 2010; Kok et al., 2018). Globally, mineral dust can directly influence the atmospheric

radiation budget and indirectly affect the radiation budget via the cloud condensation nucleus effect (e.g., Stanelle et al., 2014). Locally, mineral dust is known to affect hot, arid, and subtropical regions (e.g., Mahowald et al., 2006; 2014). However, it is increasingly recognized that dust produced at high latitudes and cold environments may extend beyond the local source area and have regional, and even global, significance (Bullard et al., 2016).

The motion of glaciers produces fine sediment (glacial flour) that is delivered via meltwater to proglacial floodplains. Then, when the glacier retreats, more land surface area with fine sediment becomes exposed to wind action, meaning that local dust emissions at high latitudes are likely to increase in a warming climate (Bullard, 2013; Simonsen et al., 2019). Once airborne, such glacial-outwash dust has a remarkably high ice-nucleating ability under conditions relevant for mixed-phase cloud formation (Tobo et al., 2019). In addition, at high latitudes, the low humidity, strong winds, permafrost, and niveo-aeolian processes promote dust emission and distribution of sediments. The subsequent dust deposition on the surface of ice sheets and glaciers can decrease ice albedo and increase subsequent glacier melting (e.g., Aoki et al., 2006; Fujita, 2007; Fujita et al., 2011; Nagorski et al., 2019).

Ice cores drilled in high-latitude regions preserve past aerosols including mineral dust (e.g., Lambert et al., 2008). The source of the mineral dust has been

studied mainly by using the isotopic method (Bory et al., 2003; Delmonte et al., 2008). Over the long term, mineral dust contributes to the glacial–interglacial cycle as a cooling factor (e.g., Seinfeld and Pandis, 1998). Dust deposited in inland Greenland mostly consists of the fine grain size (<5 μm), mainly coming from long-term transport from Asian source regions (Biscaye et al., 1997; A.-M. Bory et al., 2002; A. J. M. Bory et al., 2003; Uno et al., 2009). On the other hand, dust deposited on the Renland ice cap, a coastal region in Greenland, is dominated by coarse particles (>5 μm), suggesting a dust source local to the ice cap that sediments rapidly, typically within one day (Simonsen et al., 2019). Other regions on the Greenland ice sheet that may have significant contributions from both long-transported Asian and short-transported local sources have not been examined in detail.

Over the local scale and short-term, the picture is less clear. Few studies of deposited dust in ice cores of inland Greenland have covered the Anthropocene, especially after 2000. From a lake-sediment core in west Greenland, Salos et al., (2019) found that after 2006, the mean July air temperature shifted 1.1 °C higher. They also found that nonlinear environmental responses occurred with or shortly after the abrupt climate shift, including increases in both dust and ice-sheet discharge. However, the dating uncertainty of ice cores makes it difficult to compare an ice-core proxy such as dust with a

climatic index such as air temperature. Over the past 600 years, the warmest period began after 2000. The dust in this period has been modeled and monitored by satellite, but such approaches have been insufficient for understanding local-scale climate systems (Bullard et al., 2016). For example, satellite detection of dust is particularly challenging in the high latitudes due to darkness above the polar circles in late fall and winter (Bullard et al., 2016). Thus, a record of deposited dust from an ice core with accurate dating resolution would greatly help us evaluate the relationship between dust and the local climate system.

The Greenland ice sheet has a dome in the southeastern area (SE-Dome; 67.18°N, 36.37°W, 3170 m a.s.l.), located on the margin of Greenland ice sheet. Despite its high altitude of over 3,000 m a.s.l., the SE-Dome is located near the North Atlantic Ocean. The SE-Dome lies midway between ice-core sites in inland Greenland and Renland. Thus, the SE-Dome is an ideal location to evaluate contributions of both Asian and local sources of mineral dust. Also, due to the extremely high accumulation rate at the SE-Dome, its ice-core record has a high time resolution (Iizuka et al., 2017). Calibration between oxygen isotope ($\delta^{18}O$) data from SE-Dome samples and $\delta^{18}O$ models produced a reconstruction of the paleoclimate and atmospheric circulation over the last 60 years with an uncertainty of ±2 months (Furukawa et al., 2017). Thus, over this period, paleoclimate reconstruction here allows one to examine the relationship between

dust and climate on the seasonal scale. In this study, we analyzed dust concentrations in the SE-Dome ice core over this period, investigating the relationship between the climate system and a high-latitude dust source, with focus on the post-2000 years.

2 Materials and Methods

2.1 SE-Dome ice core and age scale

Dust data came from a 90.45-m depth ice core obtained at a dome site on the SE-Dome (67.18°N, 36.37°W, 3170 m a.s.l., Fig. 1a). The annual mean temperature at the SE-Dome is −20.9 °C, based on 20-m-deep firn-temperature measurements (Iizuka et al., 2017). For a timescale, we use the SEIS2016 age scale for 1960–2014, which is determined by the oxygen-isotope matching method (Furukawa et al., 2017). The SEIS2016 scale has been carefully evaluated with independent age markers of tritium and volcanic events, and its precision is within two months (Fig. 3 in Furukawa et al., 2017). Depths marking the beginning of the year are found by linear interpolation.

136 2.2 Microparticle (dust) concentration measurements

137 In a cold room (Institute of Low Temperature Science, Hokkaido
138 University, Japan), we divided the 90.45-m ice core into 941 sections, each of
139 close to 100 mm depth. Based on the SEIS2016 age scale, uppermost 852
140 samples cover the period from 1960 to 2014. The samples were divided using a
141 clean ceramic knife in a cold clean room (class 10000), put into clean
142 polyethylene bottles, and then were melted in the bottle at room temperature in a
143 clean room. Concentration and grain-size distributions of the microparticles,
144 hereafter dust, were measured using a Beckman Coulter Counter Multisizer 3
145 with an aperture of 30 μm (size range between 0.6 and 18 μm in diameter) in a
146 class 10000 clean room.

147 To make a measurement solution of 15 ml, we mixed 3 ml of melted ice-
148 core sample with 12 ml of a liquid dilution agent (ISOTON II, Beckman) in a 25
149 ml bottle (Accuvette ST, Beckman). To dissolve any bubbles in the melted water,
150 the solutions were kept at least 24 hours in the clean room after melting. Then,
151 to homogenize the settled (larger) particles, the solutions were gently stirred
152 using a 1000 μl pipette (Eppendorf Research) without making bubbles. For the
153 background value, we ran a blank test of the above method by using 96 samples
154 with ultra-pure water (18.2 MΩ cm). Each sample consisted of 3 ml of the super-
155 pure water and 12 ml of the diluent. The average and standard deviation of the

156 particle number and mass concentration were 1900 ± 423 ml^{-1} and 2.6 ± 1.0 μg
157 kg^{-1}, respectively. The mass concentration was calculated from dust volumes,
158 assuming a spherical approximation and a density of 2.50 g cm^{-3}.
159

160 2.3 Flux estimation

161 The annual and seasonal dust fluxes are based on the seasonal average
162 value of each dust concentration value multiplied by the seasonal accumulation
163 rate. The seasonal boundaries are March 1st, June 1st, September 1st, and
164 December 1st for spring (MAM), summer (JJA), autumn (SON), and winter (DJF).
165 The annual dust fluxes use the boundary of January 1st. These annual and
166 seasonal accumulation rates are estimated based on the SEIS2016 age scale
167 (Furukawa et al., 2017).

168 2.4 Observation of particle sizes and shapes

169 Insoluble particles were collected on a polycarbonate membrane filter
170 (Advantec 13 mm, pore size 0.4 μm) following the method in Iizuka et al. (2009).
171 The filter was coated with Pt by using magnetron sputter (MSP-10, Vacuum
172 Device). Then, the particle shape was observed using a scanning electron
173 microscope (JSM-6360LV, JEOL) with an energy dispersive x-ray spectrometer
174 (JED2201, JEOL). We confirmed that almost all measured particles contained Si,

indicating silicate minerals (dust). To determine their shapes, we examined particles in a sample from summer 1964 (depth 80.105 m) and a sample from summer 2003 (24.800 m), which had the largest dust mass concentrations in 1960–1999 and in 2000–2014, respectively.

2.5 ERA-40 and ERA-Interim reanalysis data

To evaluate climate records in the SE-Dome ice core, we used the ERA-40 (1958–2001) and ERA-Interim (1979–2014), hereafter ERA-I, reanalysis datasets produced by the European Centre for Medium-Range Weather Forecasts (ECMWF) (Uppala et al., 2005; Dee et al., 2011). The daily and monthly mean air temperature at the SE-Dome elevation (3170 m a.s.l.) were extracted from the pressure level air temperature by referring to the geopotential height, both in ERA-40 and ERA-I (Sakai et al., 2015; Furukawa et al., 2017). Daily precipitation was also retrieved from ERA-40 and ERA-I for the backward trajectory analysis. To maintain consistency between the two precipitation products for the whole period (1958–2014), the daily precipitation of ERA-40 (p_{40}) is calibrated with that of ERA-Interim (p_I) by a linear regression obtained for the period 1979–2001 ($p_I = 1.36p_{40}, R^2 = 0.862, p < 0.001$, Iizuka et al., 2018).

193 2.6 Backward trajectory analysis

194 To investigate source regions of the chemical species in the ice core,
195 transport pathways of air masses are analyzed using the HYSPLIT model (hybrid
196 single-particle Lagrangian integrated trajectory), a model distributed by NOAA
197 (National Oceanographic and Atmospheric Administration) (Stein et al., 2015).
198 We followed the backward trajectory analysis as described in Iizuka et al. (2018),
199 and set four points at 10,500 m above ground level (a.g.l.) at SE-Dome for the
200 start of the three-day backward trajectory calculation.

201

202 2.7. Remotely sensed snow-free terrain

203 To investigate how variations in the distribution of snow-free areas affect
204 dust sources during 1979 to 2008, we used a 0.05° gridded daily calibrated
205 radiance and classification product derived from the Advanced Very High
206 Resolution Radiometer (AVHRR). Details of this product are in Hori et al. (2017).
207 Product flag values are defined as snow, sea ice, bare land, open ocean, and
208 cloud. To calibrate the snow-free pixels, we used the bare land flags on the
209 Greenland region defined by DiMarzio (2007). Over a month, we counted the
210 number of days a given pixel was flagged as "bare land" and the number of days
211 it was not flagged as "cloud", then took the ratio. If the ratio exceeded 0.5, it was

212 classified "snow-free" for the month. This procedure was done for each pixel of
213 the designated area for the months from April to September. The extracted snow-
214 free pixels were projected onto Lambert's azimuthal equal-area projection to
215 calculate the areal extent. The month with maximum snow-free area (July or
216 August) is defined as the "maximum month". For the analysis, the designated
217 area was that within 65–75 °N of the east coast of Greenland (Fig. 1), the most
218 likely source region of local dust based on the backward trajectory analysis
219 (maximum area of 6.5×10^4 km^2).
220

221 **3 Results and discussion**

222 3.1 Dust concentrations

223 The average concentration of dust particle number in the SE-Dome ice
224 core over 1960–2014 is 13000 ± 6200 ml^{-1} (Table 1). (Unless otherwise noted,
225 uncertainties here are the standard deviation.) The numbers also show that the
226 concentration during 2000–2014 is 14800 ± 6880 ml^{-1}, which is almost same or
227 slightly higher than that over 1960–2014. Larger particles (over 5 μm) are smaller
228 in number, but show the same trend, almost same or slightly increasing from 9.08
229 ± 1.43 ml^{-1} for 1960–2014 to 11.5 ± 2.32 ml^{-1} for 2000–2014.

230 From the profile in Fig. 2a, the dust mass concentration has an average

value (1960–2014) of 34.2 ± 22.1 μg kg^{-1}. The average blank error is 7.6 % in this study. Table 1 shows that the average mass concentration increases after 2000 to 42.9 ± 29.1 μg kg^{-1}. Both are within 1σ, but the mass concentration is 25.4% higher after 2000, but the number concentration is only 13.8% higher. The difference is related to the relative increase of the fraction of coarser particles.

The dust size distribution by mass (green and purple in Fig. 3a) over 1960–2014 show a bimodal trend. One peak occurs around 1–2 μm, the other around 15 μm, suggesting contributions from two sources. The dust size distribution of Renland ice core (the RECAP Holocene) has a peak around 20 μm, suggesting high contribution from local source (Simonsen et al., 2019). Thus, the large particle mode (around 15 μm) of the SE-Dome ice core implies a nearby dust source. As the long-term transport from Asian source regions has particles mostly less than 5 μm (Biscaye et al., 1997; A.-M. Bory et al., 2002; A. J. M. Bory et al., 2003; Uno et al., 2009), we divide the two sources at 5 μm. The mass concentration for dust larger than 5 μm is 10.7 ± 10.8 μg kg^{-1}, which is 31.3% of the total mass concentration during 1960–2014. For the period 2000–2014, the corresponding mass for dust larger than 5 μm is 12.6 ± 12.9 μg kg^{-1}, which is 29.4% of the total mass concentration. Thus, the size distribution by mass shows a similar bimodal trend between 1960–2014 and 2000–2014, suggesting little change of the source (Asian or local) contributions between the two periods. The

periods of dust events in summers 1964 and 2003 (red and blue in Fig. 3a) have larger size distributions than those in averaged distribution (green and purple in Fig. 3), suggesting high contribution from local source during the periods.

We examined SEM micrographs of particles from summer 1964 (depth 80.105 m) and summer 2003 (24.800 m). In Fig. 2a, these years have the largest dust mass concentrations in 1960-1999 and in 2000–2014. These seasons did not have any large volcanic eruption in Iceland. The SEM analyses show that the SE-Dome ice core has a significant number of dust particles over 5 μm, especially in 2003 (e.g., Fig. 3d); however, the size distributions have similar trends for summer 1964 and summer 2003 (Fig. 3b). In addition, the dust-particle shapes, as indicated by the aspect ratios, are similar between summer 1964 and summer 2003 (Fig. 3c). The similar size distributions and aspect trends suggests the same contributions from each source region between the two seasons.

3.2 Annual and seasonal dust flux reconstructions

The annual and seasonal dust fluxes equal the product of the mass concentration with their respective accumulation rate (Furukawa et al., 2017). The resulting annual flux for 1960–2014 in Fig. 2a gives an average of 34.8 ± 13.5 mg m^{-2} yr^{-1}. This average is greater than the yearly values of 14–19 mg m^{-2} yr^{-1} at the

inland ice cores of GRIP, NGRIP, and Dye3 (Bory et al., 2003), but is less than the 57 mg m^{-2} yr^{-1} at Haus Tausen in the coastal region of north Greenland (Bory et al., 2003) and much less than the 680 mg m^{-2} yr^{-1} at Renland on an ice cap near the ice sheet (Bory et al., 2003). Over the extensive inland region of Greenland, the flux values are low and nearly uniform due to the long-distant transport over high-elevations to the ice sheet (Bory et al., 2003). On the other hand, the high dust fluxes in Haus Tausen and Renland are mainly due to the local source (Simonsen et al., 2019). The average flux value of 34.8 mg m^{-2} yr^{-1} of the SE-Dome ice core is about twice that of the inland ice cores. We argue next that this difference indicates that some dust particles come from local sources such as exposed glacial sediments, moraines, rock, soil, and sand in coastal Greenland (e.g. Bullard et al., 2016).

The high contribution to the flux from large particles is one argument for a local dust source. The average annual flux from particles larger than 5 μm is 10.6 ± 4.26 mg m^{-2} yr^{-1} (Fig. 2b, blue curve), which is 30.5% of the total flux value. Due to the relatively rapid fallout of such large particles, they must be from a nearby source. For particles smaller than 5 μm, the average annual flux is the remaining 24.2 (= 34.8 − 10.6) mg m^{-2} yr^{-1}. Of this flux, some must also be from the local sources. The similar method of the 5 μm threshold of dust size dividing long and local transportation was done in coastal Antarctica (Baccolo et al., 2018).

290 If we assume that this remaining dust flux equals that from long distance sources
291 plus fine dust from local sources, with the former equaling that reaching the inland
292 ice cores of GRIP, NGRIP, and Dye3 (14–19 mg m^{-2} yr^{-1}), then the annual flux of
293 fine particles from local sources equals 5.2-10.2 mg m^{-2} yr^{-1}. This amount from
294 local sources is 15.0-29.3% of the total flux. Totaling both the smaller and larger
295 dust flux from the local sources, we estimate that 45.5–59.8% of the dust at the
296 SE-Dome ice core is from a local source.

297 A second argument for a local source contribution comes from the recent
298 trend in annual flux. In particular, the total flux is higher after 2000 (46.6 ± 16.2
299 mg m^{-2} yr^{-1} during 2000–2014; Table 1 and Fig. 2a), but the flux from Asia is not
300 likely to have increased during this time. In particular, Liu et al., 2020 found that
301 the Asian dust intensity during 1961–2020 was high until 1980 and then
302 decreased to the present (2020). This fact suggests that the Asian dust source
303 by itself cannot explain the high flux after 2000 in the SE-Dome ice core. Given
304 that the atmospheric circulation does not change after 2000 (Fig. 1b,c), the
305 increase after 2000 must be from a local source. In addition, the annual flux of
306 the larger (>5 μm) particles also increased after 2000 to 13.3 ± 5.33 mg m^{-2} yr^{-1}
307 (2000–2014; Table 1 and Fig. 2b). Thus, the contribution from local sources
308 probably increased after 2000.

309 Finally, a third argument for a local source comes from the trend in

seasonal flux. The seasonal fluxes during 1960–2014 are plotted in Fig. 2c. We split this period into before and after 2000. Table 2 shows the averages in both periods. During 1960–1999, the averages are nearly the same for all seasons (7.19-8.24 mg m^{-2} yr^{-1}). For 2000–2014, the highest average is in autumn at 15.7 ± 8.81 mg m^{-2} yr^{-1}, suggesting that the high dust flux after 2000 was mainly driven by the increase in autumn. A similar increase in autumn flux occurs for the large particles (Fig. 2d, Table 2). In particular, the average fluxes during 1960–1999 are nearly the same for all seasons (2.21–2.45 mg m^{-2} yr^{-1}). But for 2000–2014, the highest average is in autumn at 3.72 ± 2.27 mg m^{-2} yr^{-1}. However, Asian dust storms tend to come in spring (e.g., Liu et al., 2020), and thus the increase in autumn flux is more likely due to a local source. In the next section, we suggest a cause of the increasing annual and autumn dust fluxes during 2000–2014.

3.3 Cause of the increase in annual and autumn flux after 2000

The distance that dust of a given size will travel will depend on the fallspeed of the dust, the windspeed, and the height of the dust particles. According to Tegen and Lacis (1998), dust of size 1 to 10 μm can transport in the atmosphere for only about 40 hours. To determine the sources of the dust, we calculated the air-mass distributions arriving at the SE-Dome site from back-

329 trajectory analyses going back three days. The air masses are separated into
330 those from 1000 and 1500 m a.g.l., and those from 10 and 500 m a.g.l. The latter
331 case of the two lower air masses can entrain dust emitted from the surface. Fig.
332 1 shows these lower air masses. The air masses mainly come from regions of
333 Greenland just north of SE-Dome, extending up to about 75°N, and include
334 regions just offshore as well as some coastal regions to the south. Both periods
335 between 1960–1999 and 2000–2014 have similar distribution patterns of air mass.
336 The similarity suggests that the increase in particle number during 2000–2014
337 was not driven by a change in atmospheric circulation, but by higher dust
338 emissions in the source regions. Given that the air-mass trajectories do not show
339 the emissions of dust, we focus on specific regions in the higher-probability areas
340 that are likely to have the greatest emissions. These regions would be the snow-
341 free areas in the coastal regions. Thus, we focus on the area marked in red in
342 Fig. 1a.

343 The area includes the cities of Tasiilaq and Itseqqortoormiit, where the
344 Danish Meteorological Institute (DMI) measures air temperature and precipitation.
345 Tasiilaq is located at a coastal region of southeastern Greenland (~190 km from
346 the SE-Dome site, Fig. 1a). Both annual dust fluxes during 1960–2014 correlate
347 more strongly with air temperature in Tasiilaq ($r = 0.61$ in Table 3, Fig. 4a) than
348 with that at the SE-Dome site (Table 3). Most coastal regions in southeastern

Greenland have exposed snow-free areas of rock, soil, and glacial flour, which are potential dust sources. The lower air masses, which would be the main atmospheric transport for larger dust, come from the eastern coast between 65 and 75 °N of Greenland (Fig. 1). At nearly four times the distance to Tasiilaq lies Itseqqortoormiit (Fig. 1), another potential dust source because it is also on the coast (Fig. 1a). But air temperature in Itseqqortoormiit has lower correlation with the SE-Dome dust (r = 0.35) than that of Tasiilaq. This suggests that the larger dust likely comes from very close to the SE-Dome site.

The autumn dust fluxes during 1960–2014 also have high correlations with autumn air temperature in Tasiilaq (r = 0.50 in Table 3, Fig. 4b). Even omitting the extremely high dust-flux datum from autumn 2014, the autumn average of dust flux (2000–2013) is still highly correlated to the Tasiilaq air temperature (r = 0.52). The correlation suggests that a warmer autumn on the coast increases the dust emission from snow-free areas exposed by a delay of seasonal snowpack. The seasonal snow-free area would be an additional dust source in the coastal regions, especially during autumn. Thus, high correlations between dust flux and Tasiilaq air temperature, both annual and autumn, during 1960–2014 suggest that the warming in the coastal regions of southeastern Greenland after 2000 promotes dust emission to the atmosphere.

The snow-free area trend by AVHRR during 1979–2008 is consistent with

such warming, showing a loss of seasonal snowpack in the coastal regions around southeastern Greenland. The snow-free areas of the region in September (Fig. 2c) show an increasing trend after 2000. The average snow-free area in September is 14700 ± 5600 km^2 during 1979–1999 and 21700 ± 10800 km^2 during 2000–2008. This increase suggests that the warmer summers and autumns after 2000 are causing a delay in the seasonal snowpack cover and an extension of snow-free areas. These snow-free areas have high correlation with the autumn dust flux (r = 0.49 for the maximum month, 0.60 for September in Table 3; Fig. 4c). The high correlations suggest a larger snow-free area in autumn increased the dust emission, leading to a higher dust flux in the SE-Dome ice core.

On the other hand, results in Table 3 show low correlations between dust flux and annual Tasiilaq precipitation (r = 0.17) and windspeed (r = 0.41). The Tasiilaq precipitation is a proxy of an aridity in Tasiilaq. Dust is more likely to emit from a source area under drier and windier conditions (e.g., Bullard et al., 2016). The low correlations suggest that the high dust flux after 2000 is not due to a high emission activity of the source area, but rather is due to extend dust emission area (i.e., seasonal snow-free area).

We also examined the correlations between the dust flux and other possible proxy variables. Results in Table 3 show low correlations ($|r| < 0.30$) with

389 the North Atlantic Oscillation (NAO), which is defined as the pressure difference
390 between the Azores High and the Icelandic Low. The low correlations with NAO,
391 as well as the Arctic Oscillation (AO, $|r| < 0.27$) are consistent with the larger dust
392 size distribution during 2000–2014 not being caused by a stronger atmospheric
393 circulation.

394 Thus, the evidence indicates that the Greenlandic warming produced a
395 larger regional dust emission via a larger seasonal snow-free area in coastal
396 Greenland. The air temperature after 2000 has been increasing throughout the
397 Arctic (Stocker et al., 2013) and specifically around southeastern Greenland
398 (Bjørk et al., 2012), consistent with a retreat of the Greenland ice sheet (Mouginot
399 et al., 2019). As mineral dust plays a key role in the climate system (Carslaw et
400 al., 2010; Kok et al., 2018), the increase in dust flux at the SE-Dome after 2000
401 is a potentially important way that high-latitude dust can affect the climate system.
402 Future studies about the dynamic of the Greenland ice sheet will need to take
403 into account the role of dust, since increased dust deposition implies an increased
404 radiative forcing on the surface of the ice sheet.

405

406 ### 3.4 Contribution of Iceland dust emission

407 Other than the Greenland coast, the next nearest potential dust source is

Iceland. Iceland is also a potential local source of volcanic emissions (Groot Zwaaftink et al., 2017). However, the average air-mass probability distribution from Iceland is just 1.51 ± 1.47% (Figs. 1b,c), which is less than one-third that of the 4.88 ± 2.37% value from 65 to 75 ºN of eastern Greenland by the trajectory analyses. Moreover, the fraction of air trajectories from Iceland hardly changes from the earlier period of 1960–1999 (1.53 ± 1.47%) to the recent period of 2000–2014 (1.48 ± 1.49%). Thus, the dust-flux increase after 2000 is not explained by the contribution from Iceland.

Nevertheless, over shorter terms, volcanic eruptions in Iceland have affected dust deposition in the SE-Dome region. For example, the extremely high dust flux in the autumn of 2014 (41.4 mg m^{-2} yr^{-1}) might be due to the eruption of Mt. Bardarbunga in Iceland. However, the contribution of Icelandic volcanic eruptions to dust flux into the SE-Dome ice core should depend on air mass trajectory. Over 1960–2014, seven eruptions in Iceland had a volcanic explosivity index (VEI) exceeding 3 (Table 1). The average number and mass dust concentrations of the term during these seven eruptions are 13700 ± 8270 ml^{-1} and 40.1 ± 34.6 μg kg^{-1}, respectively (Table 1). These averages are higher than the overall averages during 1960–2014, but are lower than those during 2000–2014 (Table 1). So, some volcanic events likely contribute to dust deposition in the SE-Dome region (e.g., autumn 2014); however, they cannot explain the

increase of dust flux in the SE-Dome ice core after 2000. Baddock et al. (2017) showed similar results. They found that trajectories during Icelandic volcanic seasons rarely ascend high enough to reach inland Greenland, suggesting instead that Icelandic dust has more important effects on the neighboring marine environment than on the cryosphere.

4 Conclusion

We measured particle-size distributions from an ice core in the southeastern dome in Greenland (SE-Dome), using them to reconstruct annual and seasonal dust fluxes during 1960–2014. The annual average flux over the whole period 1960–2014 was 34.8 ± 13.5 mg m^{-2} yr^{-1}, a value about twice that of inland ice cores. The later term of this period 2000–2014 had the higher annual flux of 46.6 ± 16.2 mg m^{-2} yr^{-1}. The higher flux, together with other trends, indicated that some dust in the SE-Dome region came from local sources of exposed rock, soil, and sand in coastal Greenland.

The air-mass source locations hardly changed between the terms 1960–1999 and 2000–2014, suggesting that the reason for the larger size distribution during the later term was likely a higher dust production at the source. One nearby coastal source area is Tasiilaq, which had air temperatures that correlated more

strongly to the annual and autumn dust fluxes over 1960–2014 than the air temperature in SE-Dome. A probable local source is the region surrounding Tasillaq, where many snow-free areas are found, especially during summer and autumn. In addition, the snow-free area from 65 to 75 ºN of southern and eastern Greenland, possible source areas, also was highly correlated during 1979–2008 to the autumn dust flux, especially after 2000. The high dust flux in the SE-Dome ice core after 2000 may indicate a greater influence of high-latitude dust to the future climate system.

Acknowledgements

The authors gratefully acknowledge the Air Resources Laboratory (ARL) for the provision of the HYSPLIT transport and dispersion model on the READY Web site (http://www.arl.noaa.gov/ready.html) and windspeed records at Tasiilaq by National Centers for Environmental Information (NCEI), National Oceanic and Atmospheric Administration (NOAA), U. S. (https://www.ncei.noaa.gov/), and acknowledge the Danish Meteorological Institute (DMI) for the provision of air temperature and precipitation records at Tasiilaq and Itseqqortoormiit. The paper was significantly improved as a result of comments by two reviewers and the handling by Scientific Editor Drs. S. Sandven and M. Fukasawa, to whom we are greatly indebted. We are grateful to the drilling and initial analysis teams of the

SE-Dome ice core. This study was supported by MEXT/JSPS KAKENHI Grant Numbers JP18H05292, JP26257201, and JP16H01772, and JP18H03363, and Joint Research Program and the Readership program of the Institute of Low Temperature Science, Hokkaido University. This work was partially carried out in the Arctic Challenge for Sustainability (ArCS and ArCS II) Project, Program Grant Number JPMXD1420318865, and the Environment Research and Technology Development Fund (JPMEERF20202003 and JPMEERF20205001) of the Environmental Restoration and Conservation Agency of Japan. The data used in this study will be available in the Hokkaido University Collection of Scholarly and Academic papers (http://hdl.handle.net/ 2115/67127).

References

Aoki, T., Motoyoshi, H., Kodama, Y., Yasunari, T.J., 2006. Atmospheric aerosol deposition on snow surfaces and its effect on albedo. SOLA. 2, 13-16.

Baccolo, G, Delmonte, B, Albani, S, Baroni C., Cibin G., Frezzotti M., Hampai D., Marcelli A., Revel M., Salvatore M. C., Stenni B., and Maggi V., 2018. Regionalization of the atmospheric dust cycle on the periphery of the East Antarctic ice sheet since the Last Glacial Maximum. Geochemistry, Geophysics, Geosystems 19: 3540–3554.

Baddock, M. C., Mockford, T., Bullard J. E., and Thorsteinsson T., 2017. Pathways

of high-latitude dust in the North Atlantic. Earth and Planetary Science Letters 459 (2017) 170–182

Biscaye, P., Grousset, F., Revel, M., Van der Gaast, S., Zielinski, G., Vaars, A., Kukla, G., 1997. Asian provenance of glacial dust (stage 2) in the Greenland Ice Sheet Project 2 ice core, Summit, Greenland. J. Geophys. Res. 102(C12), 26765-26781.

Bjørk, A.A., Kjær, K.H., Korsgaard, N.J., Khan, S.A., Kjeldsen, K.K., Andresen, C.S., Box, J.E., Larsen, N.K., Funder, S., 2012. An aerial view of 80 years of climate related glacier fluctuations in southeast Greenland. Nature Geoscience. 5, 427–432. https://doi.org/10.1038/NGEO1481

Bory, A.J.-M., Biscaye, P.E., Piotrowski, A.M., Steffensen, J.P., 2003. Regional variability of ice core dust composition and provenance in Greenland. Geochem. Geophys. Geosyst. 4(12), 1107. https://doi.org/10.1029/2003GC000627.

Bory, A.J.-M., Biscaye, P.E., Svensson, A., Grousset, F.E., 2002. Seasonal variability in the origin of recent atmospheric mineral dust at NorthGRIP, Greenland. Earth and Planetary Science Letters. 196(3-4), 123-134.

Bullard, J.E., 2013. Contemporary glacigenic inputs to the dust cycle. Earth Surf. Proc. Land. 38, 71-89. https://doi.org/10.1002/esp.3315.

Bullard, J.E., Baddock, M., Bradwell, T., Crusius, J., Darlington, E., Gaiero, D.,

Gasso, S., Gisladottir, G., Hodgkins, R., McCulloch, R., McKenna-Neuman, C., Mockford, T., Stewart, H., Thorsteinsson, T., 2016. High-latitude dust in the Earth system. Reviews of Geophysics. 54, 447– 485.

Cappelen, J. (Ed.), 2016. Greenland-DMI historical climate data collection 1784-2015. DMI Tech. Rep. 16-04, https://www.dmi.dk/fileadmin/user_upload/Rapporter/TR/2016/DMIRep16-04.pdf.

Carslaw, K.S., Boucher, O., Spracklen, D. V., Mann, G. W., Rae, J.G.L., Woodward, S., Kulmala, M., 2010. A review of natural aerosol interactions and feedbacks within the Earth system. Atmos. Chem. Phys. 10, 1701-1737.

Dee, D.P., Uppala, S.M., Simmons, A.J., Berrisford, P., Poli, P., Kobayashi, S., Andrae, U., Balmaseda, M.A., Balsamo, G., Bauer, P., Bechtold, P., Beljaars, A.C.M., Van de Berg, L., Bidlot, J., Bormann, N., Delsol, C., Dragani, R., Fuentes, M., Geer, A.J., Haimberger, L., Healy, S.B., Hersbach, H., Hólm, E.V., Isaksen, L., Kållberg, P., Köhler, M., Matricardi, M., McNally, A.P., Monge-Sanz, B.M., Morcrette, J.-J., Park, B.-K., Peubey, C., P. de Rosnay, Tavolato, C., Thépaut, J.-N., Vitart , F., 2011. The ERA-Interim reanalysis: configuration and performance of the data assimilation system, Q. J. Roy. Meteorol. Soc., 137, 553–597. https://doi.org/10.1002/qj.828.

Delmonte, B., Andersson, P., Hansson, M., Schoberg, H., Petit, J.-R., Basile-

527 Doelsch, I., Maggi, V., 2008. Aeolian dust in East Antarctica (EPICA - Dome
528 C and Vostok): Provenance during glacial ages over the last 800 kyr.
529 Geophysical Research Letters. 35, L07703.
530 https://doi.org/10.1029/2008GL033382.
531 DiMarzio, J.P., GLAS/ICESat 1 km Laser Altimetry Digital Elevation Model of
532 Greenland, Version 1. Boulder, Colorado USA. NSIDC: National Snow and
533 Ice Data Center. https://doi.org/10.5067/FYMKT3GJE0TM.
534 Fujita, K., 2007. Effect of dust event timing on glacier runoff: sensitivity analysis
535 for a Tibetan glacier. Hydrological Processes. 21(21), 2892-2896.
536 https://doi.org/10.1002/hyp.6504.
537 Fujita, K., Takeuchi, N., Nikitin, S.A., Surazakov, A.B., Okamoto, S., Aizen, V.B.,
538 Kubota, J., 2011. Favorable climatic regime for maintaining the present-day
539 geometry of the Gregoriev Glacier, Inner Tien Shan. The Cryosphere. 5(3),
540 539-549. https://doi.org/10.5194/tc-5-539-2011.
541 Furukawa, R., Uemura, R., Fujita, K., Sjolte, J., Yoshimura, K., Matoba, S., Iizuka
542 Y., 2017. Seasonal scale dating of shallow ice core from Greenland using
543 oxygen isotope matching between data and simulation. J. Geophys. Res.
544 Atmos. 122. https://doi.org/10.1002/2017JD026716.
545 Groot Zwaaftink, C.D., Arnalds, Ó., Dagsson-Waldhauserova, P., Eckhardt, S.,
546 Prospero, J.M., and Stohl, A., 2017. Temporal and spatial variability of

547 Icelandic dust emissions and atmospheric transport. Atmos. Chem. Phys.
548 17, 10865-10878. https://doi.org/10.5194/acp-17-10865-2017.
549 Higgins, R.W., Zhou, Y., Kim, H.-K., 2001. Relationships between El Niño-
550 Southern Oscillation and the Arctic Oscillation: A Climate-Weather Link.
551 NCEP/Climate Prediction Center ATLAS 8.
552 Hori, M., Sugiura, K., Kobayashi, K., Aoki, T., Tanikawa, T., Kuchiki, K., Niwano,
553 M., Enomoto, H., 2017. A 38-year (1978–2015) Northern Hemisphere daily
554 snow cover extent product derived using consistent objective criteria from
555 satellite-borne optical sensors. Remote Sensing of Environment. 191, 402-
556 418. https://doi.org/10.1016/j.rse.2017.01.023.
557 Hurrell, J. W., Kushnir, Y., Ottersen, G., Visbeck, M., 2003. An overview of the
558 North Atlantic Oscillation. The North Atlantic Oscillation: Climate
559 Significance and Environmental Impact, Geophys. Monogr., 134, Amer.
560 Geophys. Union, 1–35, https://doi.org/10.1029/134GM01
561 Iizuka, Y., Miyamoto, A., Hori, A., Matoba, S., Furukawa, R., Saito, T., Fujita, S.,
562 Hirabayashi, M., Yamaguchi, S., Fujita, K., Takeuchi, N., 2017. A firn
563 densification process in the high accumulation dome of southeastern
564 Greenland. Arctic, Antarctic, and Alpine Research. 49, 13-27.
565 Iizuka, Y., Uemura, R., Fujita, K., Hattori, S., Seki, O., Miyamoto, C., Suzuki, T.,
566 Yoshida, N., Motoyama, H., Matoba, S., 2018. A 60 year record of

atmospheric aerosol depositions preserved in a high accumulation dome ice core, Southeast Greenland. Journal of Geophysical Research: Atmospheres. 123. https://doi.org/10.1002/2017JD026733.

Iizuka, Y., Miyake, T., Hirabayashi, M., Suzuki, T., Matoba, S., Motoyama, H., Fujii, Y., Hondoh, T., 2009. Constituent elements of insoluble and nonvolatile particles during the Last Glacial Maximum of the Dome Fuji ice core. J. Glaciol. 55 (191), 552-562.

Kok, J.F., Ward, D.S., Mahowald, N.M., Evan, A. T., 2018. Global and regional importance of the direct dust-climate feedback. Nature Communications. 9, 241.

Lambert, F., Delmonte, B., Petit, J.R., Bigler, M., Kaufmann, P.R., Hutterli, M.A., Stocker, T.F., Ruth, U., Steffensen, J.P., Maggi, V., 2008. Dust–climate couplings over the past 800,000 years from the EPICA Dome C ice core. Nature. 452, 616–619.

Li, W., Xu, L., Liu, X., Zhang, J., Lin, Y., Yao, X., Gao, H., Zhang, D., Chen, J., Wang, W., Harrison, R.M., Zhang, X., Shao, L., Fu, P., Nenes, A., Shi, Z., 2017. Air pollution-aerosol interactions produce more bioavailable iron for ocean ecosystems. Sci. Adv. 3. https://doi.org/10.1126/sciadv.1601749.

Liu, J. D. Wu, Liu, G., Mao, R., Chen, S., Ji, M., Fu, P., Sun, Y., Pan, X., Jin, H., Zhou, Y., Wang, X., Impact of Arctic amplification on declining spring dust

587 events in East Asia. Climate Dynamics. 2020. 54, 1913–1935,
588 https://doi.org/10.1007/s00382-019-05094-4
589 Mahowald, N., Muhs, D., Levis, S., Rasch, P., Yoshioka, M., Zender, C., 2006.
590 Change in atmospheric mineral aerosols in response to climate: Last glacial
591 period, preindustrial, modern, and doubled carbon dioxide climates. J.
592 Geophys. Res. 111, D10202.
593 Mahowald, N., Albani, S., Kok, J.F., Engelstaeder, S., Scanza, R., Ward, D.S.,
594 Flanner, M.G., 2014. The size distribution of desert dust aerosols and its
595 impact on the Earth system. Aeolian Res. 15, 53 –71.
596 Mouginot, J., Rignot, E., Bjørk, A. A., Van den Broeke, M., Millan, R., Morlighem,
597 M., Noël, B., Scheuchl, B., Wood M., 2019. Forty-six years of Greenland Ice
598 Sheet mass balance from 1972 to 2018. PNAS. 116 (19), 9239-9244.
599 Nagorski, S.A., Kaspari, S.D., Hood, E., Fellman, J.B., Skiles, S.M., 2019.
600 Radiative Forcing by Dust and Black Carbon on the Juneau Icefield. Alaska.
601 124, 3943–3959. https://doi.org/10.1029/2018JD029411
602 Sakai, A., Nuimura, T., Fujita, K., Takenaka, S., Nagai, H., and Lamsal, D., 2015.
603 Climate regime of Asian glaciers revealed by GAMDAM Glacier Inventory.
604 The Cryosphere. 9, 865–880. https://doi.org/10.5194/tc-9-865-2015.
605 Saros, J. E., Anderson, N. J., Juggins, S., McGowan, Yde, J. C., Telling, J.,
606 Bullard, J. E., Yallop, M. L., Heathcote, A. J., Burpee, B. T., Fowler, R. A.,

607 Barry, C. D, Northington, R. M., Osburn, C. L., Pla-Rabes, S., Mernild, S.
608 H., Whiteford, E. J., Andrews, M. G., Kerby J. T., and Post, E., 2019. Arctic
609 climate shifts drive rapid ecosystem responses across the West Greenland
610 landscape. Environ. Res. Lett. 14 (2019) 074027.
611 Schüpbach, S., Fischer, H., Bigler, M., Erhardt, T., Gfeller, G., Leuenberger, D.,
612 Mini, O., Mulvaney, R., Abram, N. J., Fleet, L., Frey, M. M., Thomas, E.,
613 Svensson, A., Dahl-Jensen, D., Kettner, E., Kjaer, H., Seierstad, I.,
614 Steffensen, J. P., Rasmussen, S. O., Vallelonga, P., Winstrup, M., Wegner,
615 A., Twarloh, B., Wolff, K., Schmidt, K., Goto-Azuma, K., Kuramoto, T.,
616 Hirabayashi, M., Uetake, J., Zheng, J., Bourgeois, J., Fisher, D., Zhiheng,
617 D., Xiao, C., Legrand, M., Spolaor, A., Gabrieli, J., Barbante, C., Kang, J.
618 H., Hur, S. D., Hong, S. B., Hwang, H. J., Hong, S., Hansson, M., Iizuka, Y.,
619 Oyabu, I., Muscheler, R., Adolphi, F., Maselli, O., McConnell, J., and Wolff,
620 E. W., 2018. Greenland records of aerosol source and atmospheric lifetime
621 changes from the Eemian to the Holocene, Nature Communications, 9,
622 1476.
623 Seinfeld, J. H., Pandis, S. N., 1998. Atmospheric chemistry and physics: From air
624 pollution to climate change. John Wiley & Sons Inc., New York
625 Simonsen, M.F., Baccolo, G., Blunier, T., Borunda, A., Delmonte, B., Frei, R.,
626 Goldstein, S., Grinsted, A., Kjær, H. A., Sowers, T., Svensson, A., Vinther,

627 B., Vladimirova, D., Winckler, G., Winstrup, M., Vallelonga, P., 2019.East
628 Greenland ice core dust record reveals timing of Greenland ice sheet
629 advance and retreat. Nat Commun. 10, 4494.
630 https://doi.org/10.1038/s41467-019-12546-2
631 Stanelle, T., Bey, I., Raddatz, T., Reick, C., Tegen, I., 2014. Anthropogenically
632 induced changes in twentieth century mineral dust burden and the
633 associated impact on radiative forcing. J. Geophys. Res. Atmos. 119,
634 13526–13546.
635 Stein, A.F., Draxler, R.R., Rolph, G.D., Stunder, B.J.B., Cohen, M.D., Ngan, F.,
636 2015. NOAA's HYSPLIT Atmospheric Transport and Dispersion Modeling
637 System. Bulletin of the American Meteorological Society. 96(12), 2059–
638 2077. https://doi.org/10.1175/BAMS-D-14-00110.1.
639 Stocker, T.F., Qin, D., Plattner, G.-K., Tignor, M., Allen, S.K., Boschung, J., Nauels,
640 A., Xia, Y., Bex, V., Midgley, P.M. (Eds.). 2013.Climate Change 2013: The
641 Physical Science Basis. Contribution of Working Group I to the Fifth
642 Assessment Report of the Intergovernmental Panel on Climate Change.
643 Cambridge University Press, Cambridge, United Kingdom and New York,
644 NY, USA, pp.1535. https://doi.org/10.1017/CBO9781107415324.
645 Tegen, I., Lacis, A.A., 1996. Modeling of particle size distribution and its influence
646 on the radiative properties of mineral dust aerosol. J. Geophys. Res. 101,

19237-19244.

Tobo, Y., Adachi, K., DeMott, P.J., Hill, T.C.J., Hamilton, D.S., Mahowald, N.M., Nagatsuka, N., Ohata, S., Uetake, J., Kondo, Y., Koike, M., 2019. Glacially sourced dust as a potentially significant source of ice nucleating particles. Nat. Geosci. 12, 253–258. https://doi.org/10.1038/s41561-019-0314-x.

Uno, I., Eguchi, K., Yumimoto, K., Takemura, T., Shimizu, A., Uematsu, M., Liu, Z., Wang, Z., Hara, Y., Sugimoto, N., 2009. Asian dust transported one full circuit around the globe. Nature Geoscience. 2(8), 557-560.

Uppala, S.M., Kållberg, P.W., Simmons, A.J., Andrae, U., Da Costa Bechtold, V., Fiorino, M., Gibson, J.K., Haseler, J., Hernandez, A., Kelly, G.A., Li, X., Onogi, K., Saarinen, S., Sokka, N., Allan, R.P., Andersson, E., Arpe, K., Balmaseda, M.A., Beljaars, A.C.M., Van De Berg, L., Bidlot, J., Bormann, N., Caires, S., Chevallier, F., Dethof, A., Dragosavac, M., Fisher, M., Fuentes, M., Hagemann, S., Hólm, E., Hoskins, B.J., Isaksen, L., Janssen, P.A.E.M., Jenne, R., McNally, A.P., Mahfouf, J.F., Morcrette, J-J., Rayner, N.A., Saunders, R.W., Simon, P., Sterl, A., Trenberth, K.E., Untch, A., Vasiljevic, D., Viterbo, P., Woollen, J., 2005. The ERA-40 re-analysis. Q. J. R. Meteorol. Soc. 131, 2961–3012.

667 Figure and table captions

668

669 **Figure 1.** Study area and air-mass trajectories. (**a**) Locations of southeast dome
670 (SE-Dome), Tasiilaq, and Itseqqortoormiit. Blue and red shaded regions denote
671 potential snow-free areas bordering the Greenland Ice Sheet. The red regions
672 are obtained from the air-mass trajectories in Figs 1b and 1c (east coast between
673 65 and 75 °N), and used to calculate snow-free area in September (Fig. 2c). (**b**)
674 Probability distribution (%) of an air mass arriving at the SE-Dome site from a 3-
675 day, 3-D backward-trajectory analysis, averaged over 1960–1999 for air-mass
676 starting elevations 10 and 500 m a.g.l. Color scale at bottom. **(c)** Same as (b)
677 except for period 2000–2014. Probability of the air mass is weighted by the daily
678 precipitation from combined reanalysis datasets of ERA-40 and ERA-Interim.

679

680 **Figure 2.** Trends in dust mass, dust flux, and snow-free coastal area. (**a)** Annual
681 dust mass concentration (left) and dust flux (right) in the SE-Dome ice core.
682 Dotted line shows a running average over 5 years. **(b)** Same as (a) except for
683 particles exceeding 5 μm. **(c)** At left are seasonal dust fluxes in the SE-Dome ice
684 core. Blue, green, red, and purple for spring, summer, autumn, and winter,
685 respectively, the dotted lines are running averages over 5 years. At right, snow-
686 free area in September on the east coast of Greenland within 65–75ºN derived

687 from AVHRR from 1979 to 2008. (Data losses in 1980 and 1981 are due to having
688 insufficient satellite observations for that period.) **(d)** Same as (c) except for
689 particles exceeding 5 μm and without the snow-free area.
690
691 **Figure 3.** Particle distributions. **(a)** Particle mass–size distribution by the Colter
692 Counter method during 1960–2014 (purple), 2000–2014 (green), summer 1964
693 (red) and summer 2003 (blue). (**b**) Particle number–size distribution by the SEM
694 method on summer 1964 (red) and summer 2003 (blue). **(c)** Same as (b) except
695 for particles' aspect ratio. (**d**) Example of a particle larger than 5 μm from summer
696 2003.
697
698 **Figure 4.** Correlations of dust fluxes to temperature in Tasiilaq and coastal snow-
699 free area. **(a)** Annual dust flux and annual air temperature at Tasiilaq. **(b)** Autumn
700 dust flux and autumn air temperature at Tasiilaq. **(c)** Autumn dust flux and the
701 snow-free area in September during 1979–2008. Monthly air temperatures 1960–
702 2014 at Tasiilaq (65.60°N, 37.59°W) are from the Danish Meteorological Institute
703 (Cappelen, 2016).
704
705 **Table 1.** Average values and standard deviations of number and mass dust
706 concentrations during 1960–2014, 2000–2014, and seasons with large volcano

707 eruption events in Iceland. The average values and standard deviations are
708 shown in the cases of within 0.6–18 μm, and 5.0–18 μm. Seasons with 7 large
709 volcano eruption events in Iceland: 1) Bárðarbunga, autumn 2014; 2) Grímsfjall,
710 spring 2011; 3) Eyjafjallajökull, spring 2010; 4) Hekla, winter 2000; 5) Krafla,
711 autumn 1984; 6) Eldfell, winter 1973; and 7) Askja, autumn 1961.
712
713 **Table 2.** Seasonal average dust fluxes (mg m^2 $season^{-1}$) with standard deviations
714 during 1960–1999 and 2000–2014 in the cases of within 0.6–18 μm, and 5.0–18
715 μm.
716
717 **Table 3.** Annual and seasonal correlation coefficients (r) between dust fluxes and
718 potentially relevant proxies during 1960–2014. Bold marks values of 0.5 or higher.
719 Gray shading marks values from plots in Fig. 4.
720

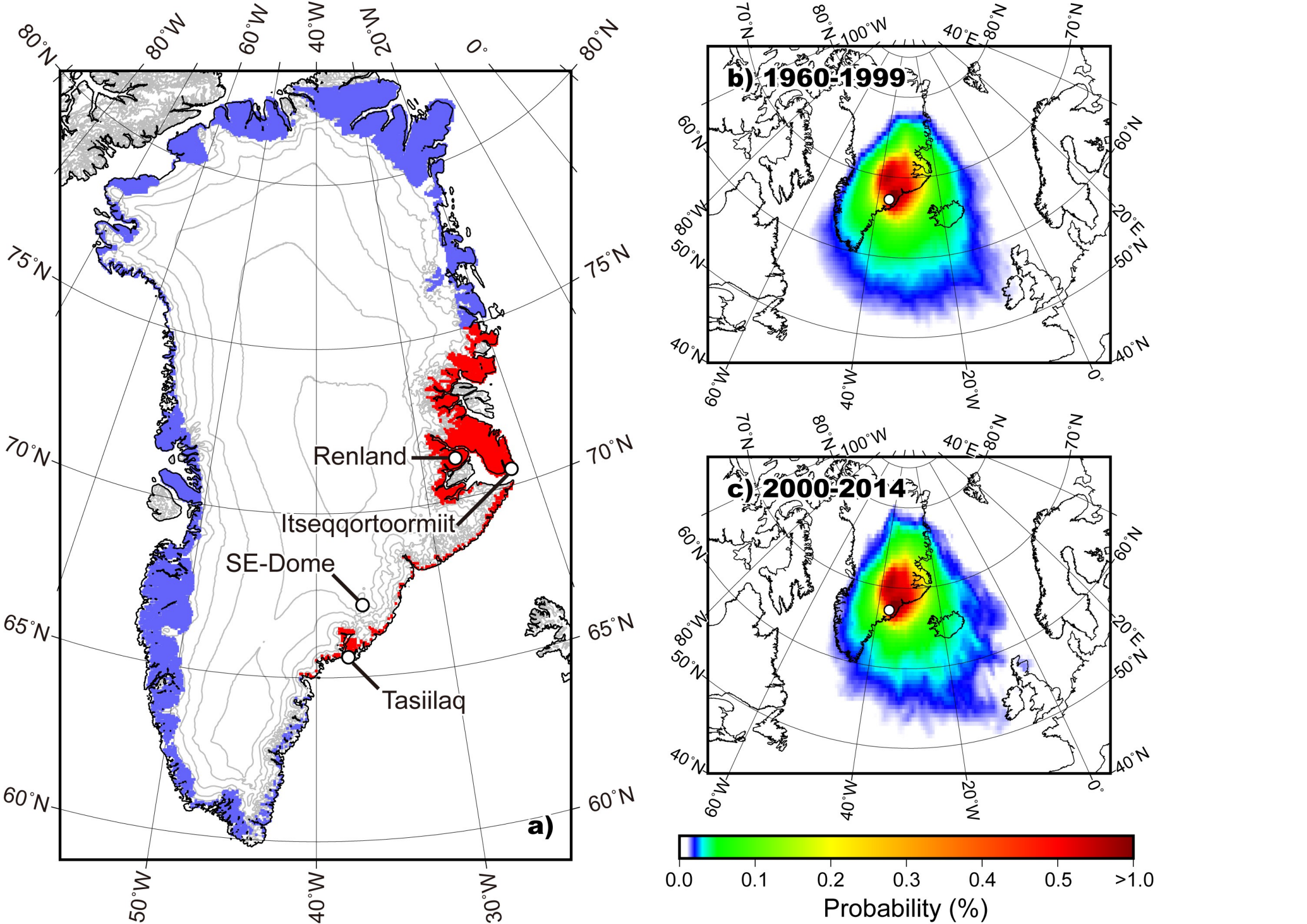
a)
b) 1960-1999
c) 2000-2014
Renland
Itseqqortoormiit
SE-Dome
Tasiilaq
0.0
0.1
0.2
0.3
0.4
0.5
>1.0
Probability (%)

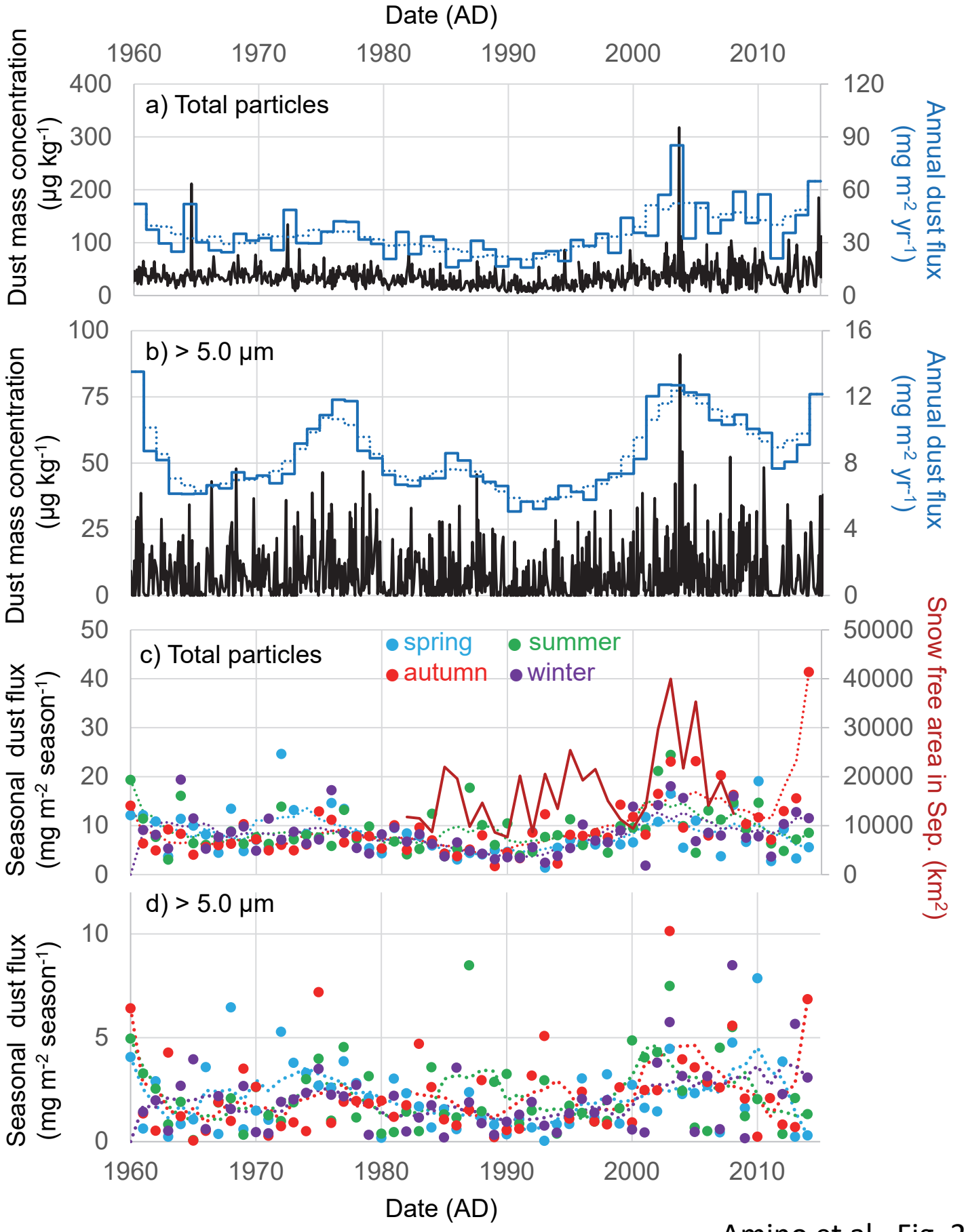

Amino et al., Fig. 2

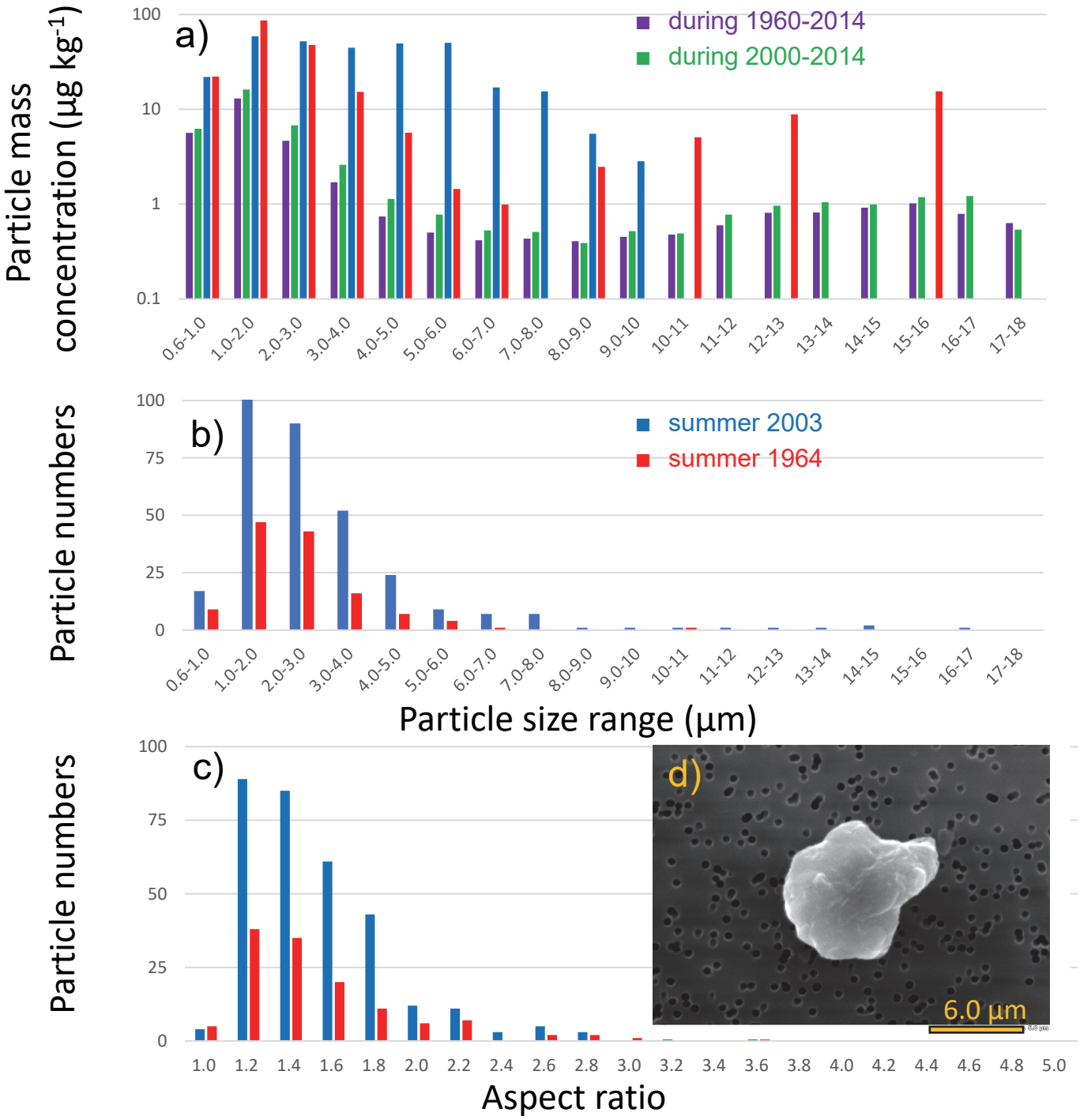

Amino et al., Fig. 3

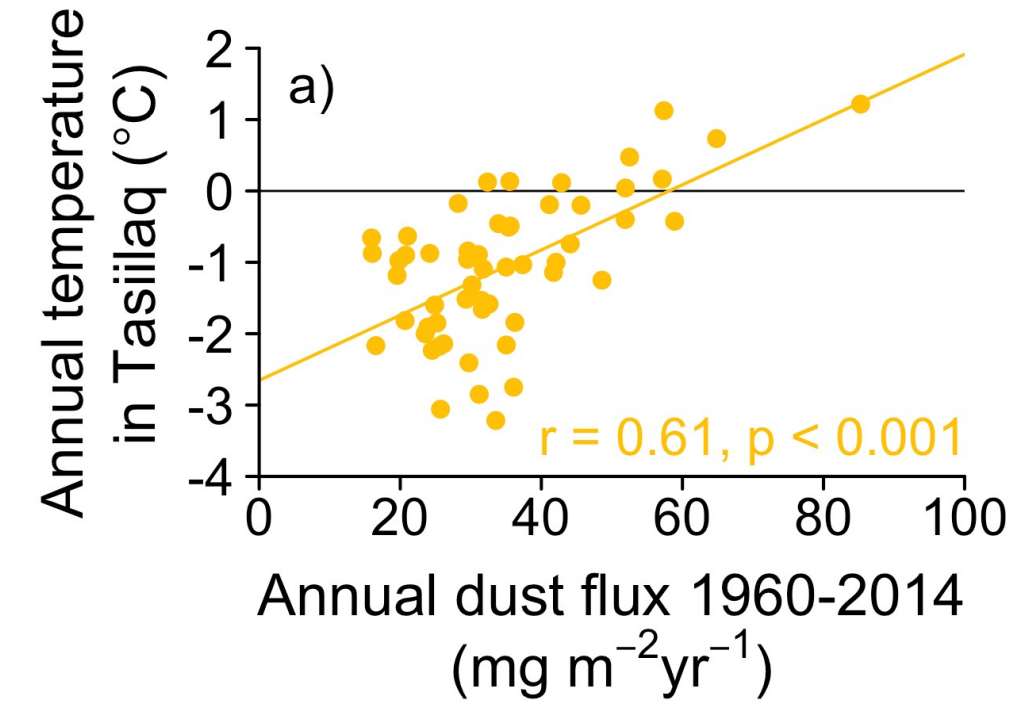
a)
Annual temperature in Tasiilaq (°C)
2
1
0
-1
-2
-3
-4
0
20
40
60
80
100
r = 0.61, p < 0.001
Annual dust flux 1960-2014
(mg m^{-2}yr^{-1})

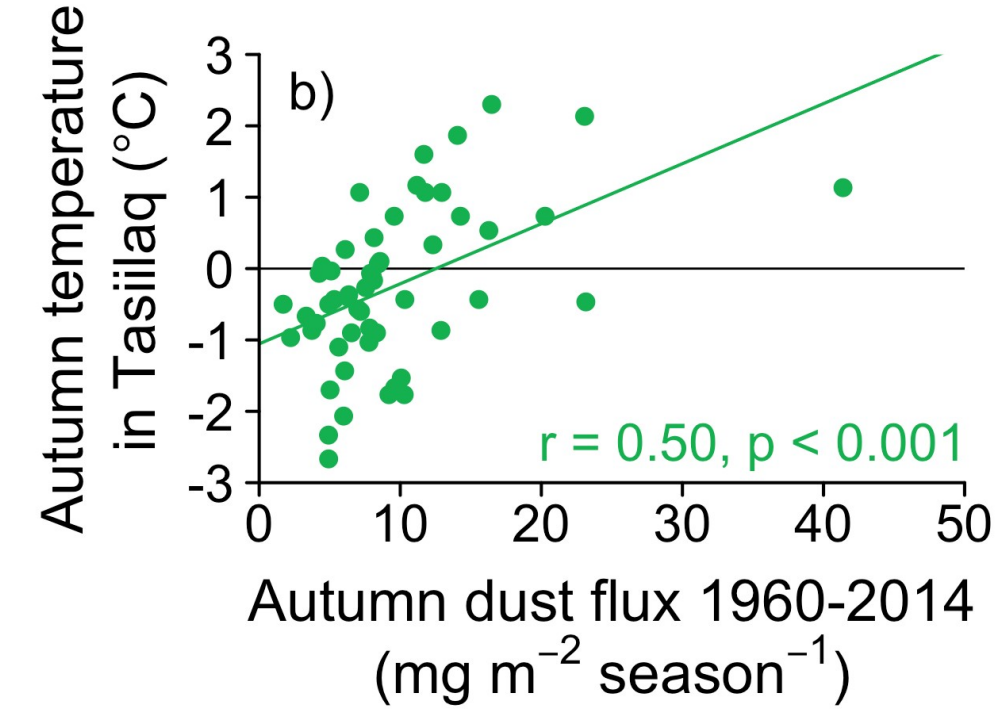
b)
Autumn temperature in Tasiilaq (°C)
3
2
1
0
-1
-2
-3
0
10
20
30
40
50
r = 0.50, p < 0.001
Autumn dust flux 1960-2014
(mg m^{-2} season^{-1})

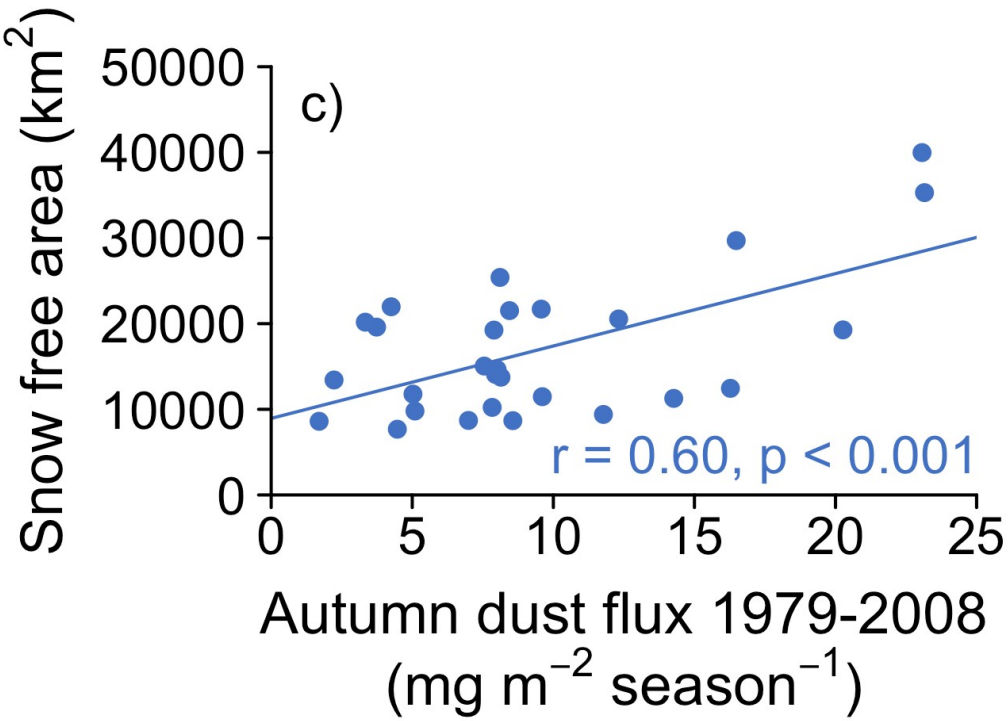
c)
Snow free area (km^2)
50000
40000
30000
20000
10000
0
0
5
10
15
20
25
r = 0.60, p < 0.001
Autumn dust flux 1979-2008
(mg m^{-2} season^{-1})

Term	Particle size (µm)
Period 1960-2014 (n =850)	0.6 ~ 18
Period 1960-2014 (n =850)	5.0 ~ 18
Period 2000-2014 (n=259)	0.6 ~ 18
Period 2000-2014 (n=259)	5.0 ~ 18
Volcanic seasons* (n=26)	0.6 ~ 18
Volcanic seasons* (n=26)	5.0 ~ 18

Number conc.(mL^{-1})	Mass conc. ($\mu g\ kg^{-1}$)
13000±6000	34.2±22.1
9.08±1.43	10.7±10.8
14800±6880	42.9±29.1
11.5±2.32	12.6±12.9
13700±8270	40.1±34.6
16.4±2.82	14.8±14.9

Period	Term	Particle size within 0.6 ~ 18 μm	Particle size within 5.0 ~ 18 μm
1960-1999	Spring	7.79 ± 4.20	2.24 ± 1.47
	Summer	8.24 ± 3.74	2.45 ± 1.71
	Autumn	7.19 ± 2.96	2.38 ± 1.89
	Winter	7.28 ± 3.44	2.21 ± 1.85
2000-2014	Spring	9.01 ± 4.73	2.86 ± 1.81
	Summer	11.2 ± 5.46	3.34 ± 2.42
	Autumn	15.7 ± 8.51	3.72 ± 2.27
	Winter	10.4 ± 4.52	3.06 ± 2.02

	Ca^{2+}	$d^{18}O$ (‰)	d-excess (‰)	NAO index	AO index	SE-Dome air temperature (ºC)	Tasiilaq air tempature (ºC)	Itseqqortoormiit air tempature (°C)	Tasiilaq precipitaion (mm)	Itseqqortoormiit precipitaion (mm)	Tasiilaq wind speed ($m\ s^{-1}$) [1974-2014]	Snow-free area (km^2) in *maximum month [1979-2008]	Snow-free area (km^2) in September [1979-2008]
Refrences	Iizuka et al., 2018	Furukawa et al., 2017	Furukawa et al., 2017	Hurrell et al., 2003	Higgins et al., 2001	Uppala et al., 2005; Dee et al., 2011	Cappelen, 2016	Cappelen, 2016	Cappelen, 2016	Cappelen, 2016	NCEI, NOAA, U. S.	This study	This study
annual [1960-2014]	**0.66**	0.27	-0.07	-0.25	-0.17	0.43	**0.61**	0.35	0.17	0.13	0.41	0.43	**0.58**
spring [1960-2014]	0.37	0.11	-0.03	-0.30	-0.05	0.39	0.20	-0.12	0.25	0.09	-0.12	0.34	0.38
summer [1960-2014]	**0.52**	0.04	-0.12	-0.03	-0.12	0.25	0.38	0.18	-0.06	-0.09	-0.16	0.25	0.30
autumn [1960-2014]	**0.83**	0.20	0.00	-0.02	-0.13	0.20	**0.50**	0.44	-0.09	0.27	0.38	0.49	**0.60**
autumn [1960-2013]	**0.65**	0.32	-0.02	-0.10	-0.05	0.22	**0.52**	0.40	-0.09	0.06	0.46	0.49	**0.60**
winter [1960-2014]	0.17	0.10	0.15	-0.17	-0.27	0.27	0.13	0.09	0.07	0.04	-0.11	0.35	0.38

* maximum month means July or August with greatest snow-free area